2020

Investigating the defects of postnatal global Fli1 deletion in a mouse model

BOSTON UNIVERSITY

SCHOOL OF MEDICINE

Thesis

INVESTIGATING THE DEFECTS OF POSTNATAL GLOBAL FLI1 DELETION IN A MOUSE MODEL

by

GRACE MARDEN

B.S., University of New Hampshire, 2012

Submitted in partial fulfillment of the

requirements for the degree of

Master of Science

2020

Approved by

First Reader

Maria Trojanowska, Ph.D.
Professor of Medicine

Second Reader

Jiyoun Kim, Ph.D.
Research Assistant Professor

ACKNOWLEDGMENTS

Thank you Maria for having the patience to encourage me to think more critically and ask important scientific questions. I know I still have a lot of work to do. Thank you Lukasz, Anda, Jaileene, Vicky, and Takashi for all of your advice and support, I would not have made it this far without you. The Pathology Laboratory Science program is made of an amazing group of people, and I am grateful to have been a part of it. Finally, thank you to my wonderful parents, Amy and Tom, and my sister Hallie. Last but not least, thank you to my fluffs, Max and Ollie.

INVESTIGATING THE DEFECTS OF POSTNATAL GLOBAL FLI1 DELETION IN A MOUSE MODEL

GRACE MARDEN

ABSTRACT

Scleroderma (SSc) is an autoimmune disease characterized by dysfunctional immunity, vasculopathy, and fibrosis of the skin and internal organs. There is a poor prognosis for SSc patients and effective therapeutics have not yet been developed. Many mouse models have been developed, but most fail to recapitulate all of the symptoms seen in SSc patients. In this study we characterize a $Fli1^{flox/flox}$ mouse with CAG Cre under the beta-actin promoter. Based on what has been previously described in mice with deletion of Fli1 in specific cell types, we predicted that global postnatal deletion of Fli1 will result in systemic fibrosis, vasculopathy, and inflammation in these mice. The penetrance of a phenotype was highly variable; however, mice that developed a phenotype displayed disorganized vascular networks, fibrosis and proinflammatory cytokines and chemokines in the skin and lungs after 4 and 8 weeks of Fli1 deficiency. Increased macrophage and dendritic cell populations were observed in the lungs after 8 weeks. $Fli1^{flox/flox}$ CAG Cre mice exhibited hair loss after 5 months of Fli1 deletion. Since our experiments focus mainly on the lungs and skin, more experiments are required to characterize these mice to determine if they can be used as a novel animal model of SSc.

TABLE OF CONTENTS

TITLE……...i

COPYRIGHT PAGE……...ii

READER APPROVAL PAGE……..iii

ACKNOWLEDGMENTS iv

ABSTRACT..... v

TABLE OF CONTENTS..... vi

LIST OF TABLES..... viii

LIST OF FIGURES ix

LIST OF ABBREVIATIONS..... xi

INTRODUCTION 1

METHODS 9

RESULTS 18

Generation of $Fli1^{flox/flox}$ CAG Cre Mice 18

Vasculopathy in $Fli1^{flox/flox}$ CAG Cre Mice 20

Fibrosis in $Fli1^{flox/flox}$ CAG Cre Mice 21

Immune dysregulation in $Fli1^{flox/flox}$ CAG Cre Mice 27

DISCUSSION..... 35

REFERENCES 38

CURRICULUM VITAE 42

LIST OF TABLES

Table	Title	Page
1	Mouse qPCR Primers	17

LIST OF FIGURES

Figure	Title	Page
1	SSc Pathogenesis	2
2	Fli1 in mouse embryogenesis	4
3	TGFβ Signaling on Fli1	4
4	Classification of mouse models of SSc	7
5	$Fli1^{loxP/loxP}$ CAG Cre Mouse Generation	18
6	Fli1 Expression	19
7	Vascular Permeability with Evans Blue	20
8	Trichrome Skin	21
9	Profibrotic gene expression in the skin	23
10	Trichrome Lung	24
11	Profibrotic gene expression in the lung	25
12	Picrosirius Red Stain Heart	26
13	H&E Lung	27
14	IHC anti-CD45 Lung	28
15	Immune cell populations in the lung	29
16	Proinflammatory gene expression in the lung	30
17	Proinflammatory gene expression in the skin	31
18	Hair Loss	32

19 Trichrome in the Skin after 5 Months 33

20 H&E in the Skin after 5 Months 34

LIST OF ABBREVIATIONS

α-SMA ..... alpha-Smooth Muscle Actin

ACK ..... Ammonium-Chloride-Potassium

APES ..... Aminopropyltriethoxy Silane Solution

CCL2 ..... C-C Motif Chemokine Ligand 2

CCL7 ..... C-C Motif Chemokine Ligand 7

CD45 ..... Cluster of Differentiation 45

CD163 ..... Cluster of Differentiation 163

Colα1 ..... Collagen Type 1, alpha 1 chain

Co3α1 ..... Collagen Type 3, alpha 1 chain

Co5α1 ..... Collagen Type 5, alpha 1 chain

CTA ..... Carboxy-terminal Transcriptional Activation

CX3CL1 ..... C-X3-C Motif Chemokine Ligand 1

CXCL1 ..... C-X-C Motif Chemokine Ligand 1

CXCL10 ..... C-X-C Motif Chemokine Ligand 10

DAMPs ..... Damage Associated Molecular Patterns

dcSSc ..... Diffuse Cutaneous Systemic Sclerosis

DNA ..... Deoxyribonucleic Acid

EB ..... Evans Blue

EC ..... Endothelial Cell

ECM ..... Extracellular Matrix

EDTA ..... Ethylenediaminetetraacetic Acid

EndoMT ..... Endothelial to Mesenchymal Transition

ETs ..... E-Twenty-Six

Etv2 ..... ETs Variant 2

FACS ..... Fluorescent Activated Cell Sorting

FB ..... Fibroblast

FBS ..... Fetal Bovine Serum

FGFR1 ..... Fibroblast Growth Factor Receptor 1

Fli1 ..... Friend Leukemia Integration 1

FLP1 ..... Flippase-1

H&E ..... Hematoxylin and Eosin

HCl ..... Hydrochloric Acid

HIF1α ..... Hypoxia-Inducible Factor 1 alpha

HIF1β ..... Hypoxia-Inducible Factor 1 beta

IFI44 ..... Interferon Induced Protein 44

IFNβ ..... Interferon beta

IL1β ..... Interleukin 1β

IL6 ..... Interleukin 6

IL10 ..... Interleukin 10

ILD ..... Interstitial Lung Disease

IP ..... Intraperitoneal

KOMP ..... Knockout Mouse Project

lcSSc ..... Limited Cutaneous Systemic Sclerosis

MMP9 ..... Matrix Metallopeptidase 9

MMP12 ..... Matrix Metallopeptidase 12

mRNA ..... Messenger RNA

MX1 ..... MX Dynamin Like GTPase1

PAH..... Pulmonary Hypertension

PAMPs ..... Pathogen Associated Molecular Patterns

PBS ..... Phosphate Buffered Saline

PCAF..... P300/CBP-associated Factor

PCR ..... Polymerase Chain Reaction

PDGFRα..... Platelet Derived Growth Factor Receptor alpha

PDGFRβ..... Platelet Derived Growth Factor Receptor beta

PECAM-1 ..... Platelet Endothelial Cell Adhesion Molecule-1

PKC-δ..... Protein Kinase C-delta

PRRs ..... Pattern Recognition Receptors

RNA ..... Ribonucleic Acid

SLE ..... Systemic Lupus Erythematosus

SSc ..... Systemic Sclerosis

TE..... Tris-EDTA

TGF-β..... Transformation Growth Factor-beta

TGF-β1..... Transformation Growth Factor-beta (isoform)

TGF-β2..... Transformation Growth Factor-beta 2 (isoform)

TGF-β3..... Transformation Growth Factor-beta 3 (isoform)

TIMP1 ..... TIMP Metallopeptidase Inhibitor 1

TNFα.....Tumor Necrosis Factor alpha

VEGFR2 ..... Vascular Endothelial Growth Factor Receptor 2

INTRODUCTION

Systemic Sclerosis

Systemic sclerosis (SSc), or Scleroderma, is a multi-organ autoimmune connective tissue disease with high morbidity and mortality, for which there are no effective therapies [1]. Hallmarks of SSc include immune dysfunction, vasculopathy, and excessive fibrosis of the skin and internal organs, and it most commonly effects women in their forties and fifties [1,2]. Patients are classified as either limited (lcSSc) or diffuse (dcSSc) based on the extent of cutaneous involvement; while helpful to predict disease progression and potential clinical complications, this classification is far from ideal [1,3]. Even though both groups seem to have distinct disease manifestations, there are SSc patients that cannot be characterized by this dichotomous categorization [3]. Amongst the most serious complications, interstitial lung disease (ILD), and pulmonary hypertension (PAH) are the leading cause of death in SSc [1]. Recent studies also implicate cardiomyopathy with myocardial fibrosis and diastolic dysfunction as a poor predictor of survival [1,4]. Environmental factors are likely to be involved in the initiating event and disease progression, likely acting on a permissive genetic background [2].

SSc Etiology and Pathogenesis

The etiology of SSc is unknown, however, early insult to microvasculature promotes sustained innate and adaptive immune involvement, subsequent inflammation, and exacerbated fibrosis [5]. The sensitivity of endothelial cells makes them susceptible to various injurious stimuli, which could result in EC activation, apoptosis, or endothelial to mesenchymal transition (EndoMT); EndoMT is the change in phenotype from an

endothelial to mesenchymal cell [2]. EndoMT has been implicated in the pathogenesis of SSc due to the observation of this transformation occurring in pulmonary and dermal vessels in SSc patients [6]. Stromal progenitors, FBs, ECs, pericytes and dermal adipocytes have the ability to transform into an alpha-smooth-muscle (α-SMA) expressing, collagen-producing cell type, contributing to the pathogenesis of SSc [1,2]. Raynaud phenomenon is the initial clinical manifestation of SSc, supporting the involvement of the vascular compartment early in disease pathogenesis [2]. Immune dysregulation also plays an important role, with both innate and adaptive immunity being involved [2]. These alterations ultimately lead to persistent fibroblast activation and ECM deposition [2].

A

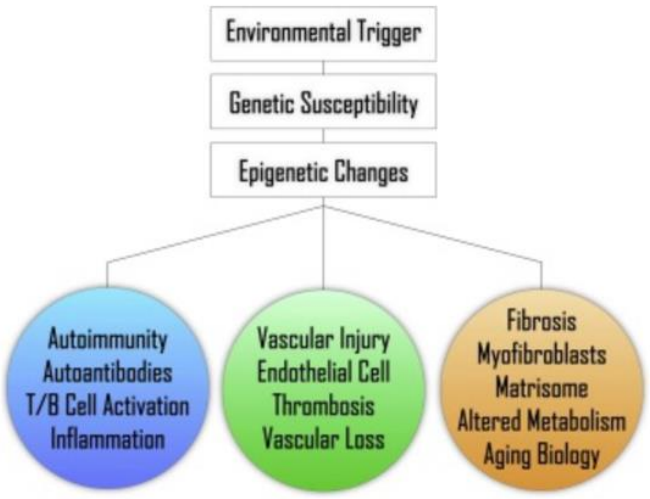

B

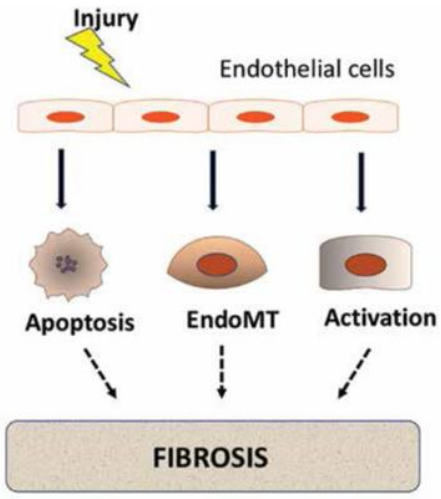

Figure 1: SSc Pathogenesis A) The triad underlying the clinical manifestations of SSc [1]. B) Injury to endothelial cells can result in several mechanisms including apoptosis, EndoMT, and activation of fibroblasts which all contribute to fibrosis in SSc [2].

Transcription Factor Fli1

Friend leukemia integration 1 (Fli1) is expressed in endothelial cells, immune cells, keratinocytes and fibroblasts [7]. As part of the E-twenty six (ETs) family of transcription factors that have a conserved DNA binding domain, Fli1 binds a core 5'-GGAA/T-3' consensus sequence [8]. The transcriptional activity of Fli1, whether activation or suppression, is influenced by the carboxy-terminal transcriptional activation (CTA) domain [9]. Fli1 is expressed early on in vascular endothelium and hematopoietic stem cells, where it serves crucial roles [7]. During embryogenesis, ETs variant 2 (Etv2) binds to the promoter region of Fli1 and activates its expression along with other genes responsible for vasculogenesis. The Fli1 protein is able to sustain its gene expression by binding to its own promoter region for continued support of vascular integrity [10]. Mice with homozygous Fli1 gene die during embryogenesis due to disrupted vasculature [2]. Data from our laboratory demonstrates a role for Fli1 in maintaining vascular homeostasis [11]. Aberrant Fli1 expression is seen in several autoimmune diseases and likely contributes to their pathogenesis [12]. In vitro studies reveal that epigenetic modifications to the Fli1 gene in fibroblasts also control cellular events preceding the fibrotic phenotype via enhanced promoter methylation in SSc fibroblasts [13]. Fli1 expression is markedly decreased in vivo in lesional and non-lesional skin of SSc patients [12,14].

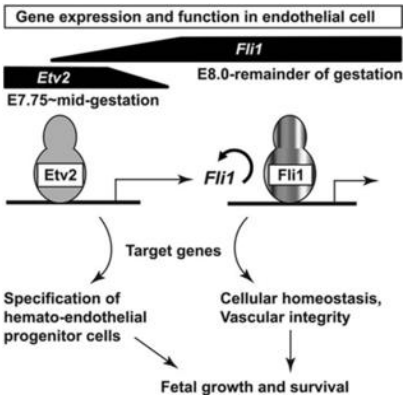

Figure 2: Fli1 in mouse embryogenesis
Timing and control of Fli1 in mouse embryogenesis. Fli1 regulates vascular morphogenesis and integrity early on in mouse development [10].

Fli1 and SSc Fibrosis

ETs transcription factors have been identified as contributors of extracellular matrix (ECM) remodeling; in particular, Fli1 was found to suppress type I collagen expression in human dermal FBs by several mechanisms [2, 15]. Type I collagen is the most abundant component of the ECM, and SSc patients exhibit exaggerated deposition of collagen in the skin and internal organs [16]. Transformation growth factor (TGF)-β signaling is a major contributor to SSc fibrosis, by controlling the transcriptional activity through a cascade of post-translational modifications in FBs [16-18].

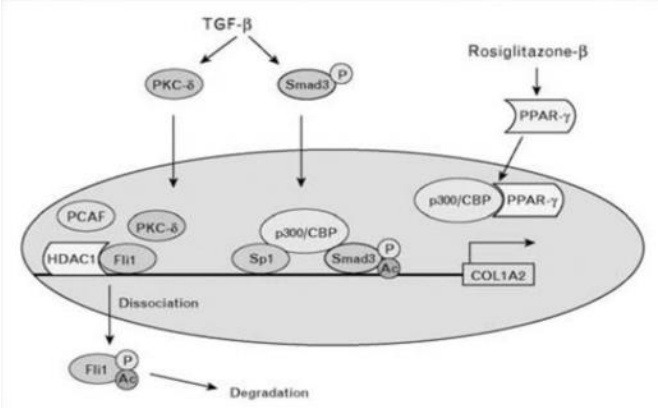

Figure 3: TGF-β signaling on Fli1
TGF-β signaling causes PKC-δ translocation to the nucleus where it phosphorylates Fli1; subsequent acetylation of Fli1 by PCAF results in Fli1 dissociation from DNA and de-repression of collagen gene transcription [18].

TGF-β isoforms are secreted by various cells types and stimulate migration, reactive oxygen species formation, collagen secretion and trans-differentiation [2]. Fibroblasts are tissue-resident mesenchymal cells that synthesize and can degrade ECM; in SSc, activated fibroblasts overproduce ECM macromolecules, being influenced by cell-cell contact, hypoxia, reactive oxygen species, signaling mediators, and changes occurring within the ECM [2]. The decrease in collagen degradation paired with the increase in activated fibroblasts and cells undergoing EndoMT leads to pathogenic fibrotic manifestations [2]. In previous studies, reduction of Fli1 in mouse dermal fibroblasts resulted in increased connective tissue growth factor (CTGF), type I collagen production and reduction of matrix metalloproteinases [9].

Fli1 and SSc Vasculopathy

SSc vasculopathy can be described as progressive structural damage of capillaries leading to reduced capillary density and blood flow [2]. ECs are highly responsive to stimuli and play an important role in regulating blood flow and immune responses by modulating expression of adhesion molecules and genes responsible for vascular permeability; they secrete proinflammatory cytokines and chemokines in response to injury [4]. Fli1 is markedly decreased in the ECs of SSc patients, and due to the importance of Fli1 in maintaining vascular homeostasis by regulation expression of EC cell markers like VE-cadherin and platelet endothelial cell adhesion molecule (PECAM)-1, we expect that the depletion of Fli1 is mainly responsible for the development of vascular abnormalities [11]. Mice with conditional deletion of Fli1 in endothelial cells show a disorganized, fragile vascular networks, and decreased expression of VE-cadherin and PECAM-1,

similar to those seen in SSc patients [5,11]. It was also found in SSc ECs, neuropilin-1, a co-receptor of vascular endothelial growth factor receptor (VEGFR)-2 that is transcriptionally controlled by Fli1, was decreased contributing to an anti-angiogenic program [2].

Fli1 and SSc Autoimmunity

Chronic inflammation typically results in fibrosis [1]. Innate immune responses in SSc involve damage associated molecular patterns (DAMPs) interaction with pattern recognition receptors (PRRs), activation of macrophages, mast cells and dendritic cells. The adaptive immune response helps to sustain chronic inflammation [1]. Th_2 and Th_{17} T-cell subsets predominate in early stages of disease, which in turn contributes to the activation of macrophages to a profibrotic phenotype, secreting interleukin (IL)-10 and TGF-β [19]. In SSc biopsies, macrophages expressing profibrotic markers were found in perivascular regions as well as between thickened collagen bundles [20]. Fli1 was found to regulate development of immune cells of myeloid lineage in mice; by functionally deleting the CTA domain from Fli1 in a mouse model; increased populations of monocytes, macrophages and dendritic cells were seen in the bone marrow, spleen, and peripheral blood [21]. A recent study found that monocytes isolated from SSc patients showed decreased Fli1 levels when compared with healthy controls. In vitro studies, in which conditioned media from macrophages with depleted Fli1 was used in culture with human dermal fibroblasts, showed increased type I collagen expression, confirming the involvement of immune cells in fibrosis [Bujor, et al. In Review].

Current Limitations in SSc Research

There are many animal models of SSc, but they fail to reflect the genetic component of the disease [22]. Transgenic models have not been able to capture the fibrotic, immune, and vascular aspects of this disease in a single setting, and the use of exogenous substances, like bleomycin, are commonly used to induce a phenotype [22]. Existing models of SSc have led to the development of therapies, but the clinical efficacy remains highly variable, as the in vivo models do not sufficiently replicate the disease [2,22]. Pathophysiological aspects of SSc can be simulated in different models of the disease

	Fibrotic site	Vasculopathy	Inflammation
Spontaneous genetic models			
Tsk1/+ mouse[5,8,11]	Dermis	Cardiomyopathy and abnormal vascular tone	Absent
Tsk2/+ mouse[29,31,32]	Dermis	Absent	Modest inflammation
UCD-200 chicken[35,37]	Skin and organs	Vascular occlusion	Perivascular infiltrate
Inducible models			
Bleomycin model[51–53]	Skin and lung	Present	Peaks between days 3 and 5, then declines
Hypochlorous model[71,73]	Skin and lung	Vasculopathy of small renal arteries	Present in the dermis
Sclerodermatous GVHD[78]	Skin	Present	Inflammation and cytokine perturbations
Angiotensin II model[79,80]	Present	Present, also has cardiovascular remodeling	Perivascular inflammation
DNA topoisomerase I and CFA[83]	Skin and lung	Not reported	Cytokine perturbations and inflammation peaks at 8 weeks

	Fibrotic site	Vasculopathy	Inflammation
Transgenic models			
Endothelin-1[87,88]	Kidney and lung	Reduced	Present
FRA-2[95,96]	Skin and lung	Present	Present
Type I TGF-β receptor[97]	Dermis	Present	Absent
Kinase-deficient type II TGF-β receptor[102,104]	Dermis and lung	Absent but addition of a VEGFR inhibitor promoted vasculopathy	Not reported
PDGFR-α[107]	Skin and organs	Not reported	Cytokine perturbations
Knockout models			
Caveolin-1[110,111,180]	Dermis	Present	Increased inflammatory responses
Egr-1[119]	Reduced fibrosis	Not reported	Reduced inflammation
Fli1[123]	Skin	Present	Not reported
MCP-1[124]	Reduced fibrosis	Not reported	Reduced inflammation
mPGES-1[128]	Reduced fibrosis	Not reported	Reduced inflammation
PPARγ[131]	Dermis	Not reported	Increased inflammation
PTEN[136]	Dermis	Not reported	Not reported
Relaxin[139]	Skin	Not reported	Not reported

Figure 4: Classification of mouse models of SSc. Table indicating the involvement of fibrosis, vasculopathy, and inflammation in existing mouse models of SSc; organized by spontaneous genetic models, inducible models, transgenic models and knockout models [modified from 23]

The Fos-related antigen-2 (FRA-2) transgenic mouse model develops many of the features of SSc [23]. Fra-2 is overexpressed in the skin and lungs of SSc patients, and mice with overexpression of Fra-2 develop fibrosis in the skin and lungs, as well as microangiopathy and immune involvement [22,23]. EC apoptosis precedes the vascular phenotype in these mice and the expression of Fra-2 is independent of TGF-β [23], suggesting that although the phenotype seems representative of SSc, mechanistically, it may not represent all of the contributors to disease pathogenesis.

Fli1$^{flox/flox}$ CAG Cre Mice

Due to the involvement of Fli1 in immune cell development, FB and EC homeostasis, we propose a mouse model, in which we utilize the global postnatal deletion of Fli1. We utilized a tamoxifen inducible Cre-recombination system driven by the beta actin promoter coupled with the cytomegalovirus early enhancer to delete floxed exon 3 of Fli1. Cre recombinase under the control of the beta actin promoter ensures the widespread deletion of functional Fli1 in cells and tissues. In this study, we aim to characterize these mice to determine if they can serve as a novel transgenic mouse model in SSc research, to aid in the development of more effective therapeutic strategies.

METHODS

Transgenic Mouse Generation

All experimental procedures were conducted in accordance with the guidelines of the National Institute of Health and were approved by the Boston University Animal Care and Use Committee. A Fli1 targeting vector purchased from the KOMP Repository was used to generate floxed Fli1 mice. 129 Agouti embryonic stem cells with the inserted KOMP vector were generated at the Transgenic Mouse Core at Harvard Medical School (Boston, MA) and used for blastocyst injection to generate chimeric mice, which were then selected for germline transmission. Heterozygous mice harboring the targeted gene mutation were crossed with transgenic C57BL/6J mice expressing FLP1 recombinase (Flpe) in all tissues, under the β-actin promoter (transgenic B6.Cg-Tg(ACT*Flpe*) 9205Dym/J, available from the Jackson Laboratory, USA, Stock number 005703). The $Fli1^{flox/flox}$ mice were crossed to C57BL/6 mice for 8 generations. Mice expressing Cre recombinase under the chicken β-actin promoter coupled with the cytomegalovirus (B6.Cg-Tg9CAG-cre/Esr1*)5Amc/J) immediate-early enhancer were purchased from the Jackson Laboratory (Bar Harbor, ME) (Stock number 004682) and crossed with $Fli1^{flox/flox}$ mice. Tamoxifen-inducible Cre-mediated recombination in these mice results in the deletion of Fli1 in widespread cells and tissues. Heterozygous CAGCre males with $Fli1^{flox/flox}$ were bred with females with $Fli1^{flox/flox}$ to produce viable experimental animals. All mice with CAGCre were heterozygous for the Cre transgene.

DNA Isolation

Genomic DNA was isolated from 2mm tail biopsies from 21-day old mice. Biopsies were incubated overnight at 55 °C in DNA digestion buffer (50 mM Tris-HCL pH 8.0, 100 mM EDTA pH 8.0, 100 mM NaCl, 1 % SDS) with a final concentration of proteinase K at 0.5 mg/mL. Neutralized phenol/chloroform/iso-amyl alcohol (25:24:1) was added and mixed for one hour at room temperature. After carefully separation of the aqueous phase, DNA was precipitated using 100 % ethanol. DNA was washed in 70 % ethanol and resuspended in 1X TE buffer (1 M Tris pH 8.0, 0.5 M EDTA pH 8.0).

Fli1loxP CAGCre (ER^{t2}) Genotyping

PCRs were performed with ~200 ng of genomic DNA, 1X PCR buffer, 3.0 mM Mg^{2+} (Bioline), 300 uM dNTPs (New England Biolabs, Ipswich, MA), 1.5 U ChoiceTaq Blue DNA Polymerase (Thomas Scientific), 100 uM primer Fli1-3loxPF5 (5'-GACTCAAACCAGGGAAAGTTGC-3'), 100 uM primer Fli1-3loxPR5 (5'-TTGGGAAGGTGGAATCTAGCAG-3'). 100 uM primer Fli1loxP-2nd5F (5'-ACCTTTGCTCCACACATCTGA-3') and 100 uM primer Fli1loxP-2nd5R (5'-ACCTTGGTTACAGGACTGAGTG-3') were used in a separate reaction to confirm the presence of both loxP sites flanking exon 3 of Fli1. Reactions were incubated at 94 °C for 3 min, then cycled 40 times (94 °C for 30 sec, 12 °C for 1 min, 72 °C for 1 min) followed by a 2 min extension at 72 °C. Reactions were separated on a 2 % agarose gel and visualized with ethidium bromide. 100 uM primer CAGCreF (5'-AGGCAGCTCACAAAGGAACAAT-3'), 100 uM primer CAGCreR (5'-TCGTTGCATCGACCGGTAA-3'), 100 uM primer CAGCtrlF (5'-

CTAGGCCACAGAATTGAAAGATCT-3'), and 100 uM primer CAGCtrlR (5'-GTAGGTGGAAATTCTAGCATCATCC-3') were used in one PCR reaction. Heterozygous mice produced a 300 bp transgene product and a 324 bp internal positive control, while wild type mice produced a 324 bp internal positive control product.

Tamoxifen Administration

Tamoxifen (Sigma-Aldrich, St. Louis, MO) was dissolved in sterile corn oil at a concentration of 20 mg/ml by shaking overnight at 37 °C and then stored protected from light at 4 °C. Injection doses were determined by weight, mice 4 – 6 weeks of age received intraperitoneal (IP) injections 75 mg/kg body weight or 100 mg/kg body once every 24 hours for 5 consecutive days. Mice were euthanized for organ harvest 10 days, 4 weeks, 8 weeks and 5 months days following the last injection.

Vascular Permeability

Mice were intravenously administered sterile 0.5 % Evans Blue (EB) in 1X PBS through a lateral tail vein injection. 30 min following injection, mice were euthanized with CO^2 and cervical dislocation. Skin was photographed to evaluate vascular permeability.

Gene Expression Analysis (RT-qPCR)

Tissue was stored in RNAlater (Invitrogen, Carlsbad, CA) solution at -80 °C until RNA isolation. Total tissue RNA was isolated using the RNeasy Fibrous Tissue Mini Kit (Qiagen, Hilden, Germany). 1 ug was reverse transcribed with random hexamers and the Transcriptor First Strand cDNA synthesis kit (Roche Applied Science, Penzberg, Germany) according to the manufacturer's protocol. Real-time PCR was performed using the StepOnePlus Real-Time PCR system (Applied Biosystems, Foster City, CA). The 10

ul amplification mixture contained 1 ul of complementary DNA, 0.5 mM of each primer, and 5 ul of SYBR Green PCR Master Mix (Applied Biosystems, Foster City, CA). The $2^{-\Delta\Delta CT}$ method was used to evaluate relative changes in the levels of genes of interest. Primers are listed in Table 1.

Western Blot

For western blot, whole tissue was subjected to mechanical disruption using the Tissue Lyser II (Qiagen, Hilden, Germany) in a lysis buffer containing 150 mM NaCl, 1 % Triton X-100, 50 mM Tris-HCl pH 8.0, 0.5 % sodium deoxycholate, 0.1% sodium dodecyl sulfate, and proteinase inhibitor cocktail (Roche Applied Science, Penzberg, Germany). Protein extracts were subjected to SDS-PAGE and transferred to nitrocellulose membranes. Membranes were incubated overnight at 4 °C with primary antibodies, washed in TBS containing 0.01% Tween 20, TBS-T) and incubated with the appropriate horse-radish peroxidase-conjugated secondary antibody for 1 hour at room temperature. After washing in TBS-T, visualization was performed by using enhanced chemiluminescence (ECL; Pierce, Waltham, MA). The following antibodies were used: anti-Fli1 (Abcam), at a dilution of 1:1000, and a control mouse β-actin (Sigma, St. Louis, MO) was used at a 1:5000 dilution.

Trichrome Stain

Tissue were deparaffinized and hydrated using HistoClear (National Diagnostics, Atlanta, GA) clearing agent and a graded alcohol series. Staining for 4 week and 8 weeks samples was done using a kit (Thermo Scientific, Waltham, MA) according to the manufacturer's protocol. Briefly, sections were incubated in Bouin's solution at 60 °C for one hour.

Washed in water. Incubated in working hematoxylin solution for 10 minutes. Washed in water. Stained in trichrome stain for 15 minutes. Washed in water, dehydrated in ethanol and cleared before mounting. Slides were imaged using the Olympus FlouView FV10i confocal microscope (Olympus, Waltham, MA). For 5 month skin sections, trichrome stain was performed by iHISTO (Woburn, MA) and viewed using CaseViewer2.3.

Hematoxylin and Eosin Stain

Tissue were deparaffinized and hydrated using HistoClear (National Diagnostics, Atlanta, GA) clearing agent and a graded alcohol series. Slides were incubated in Gill's Hematoxylin for 2 minutes, washed twice in water, and incubated in 0.3% ammonia hydroxide for 1 minute. Sections were washed in water and incubated in 75% ethanol, followed by 95% ethanol for 2 minutes each. Incubation in Eosin Y solution lasted for 30 seconds before dehydrating, clearing, and mounting. Slides were imaged using the Olympus FlouView FV10i confocal microscope (Olympus, Waltham, MA). For 5 month skin sections, trichrome stain was performed by iHISTO (Woburn, MA) and viewed using CaseViewer2.3.

Picrosirius Red Stain

Tissue were deparaffinized and hydrated using HistoClear (National Diagnostics, Atlanta, GA) clearing agent and a graded alcohol series. Fixation was achieved with incubation in Bouins' solution (Fisher, Hampton, NH) at 55 °C for 1 hr. A 10 min incubation in 0.1 % Fast green (Fisher F-99) is followed by a 1 % acetic acid wash. Sections were washed in water and incubated in 0.1% Sirius red (Sigma 0-0303) for 30min. Tissue sections were dehydrated in an ethanol series and cleared in HistoClear before mounting. Slides were

imaged using the Olympus FlouView FV10i confocal microscope (Olympus, Waltham, MA).

Immunohistochemistry

Immunohistochemistry was performed on 4 % paraformaldehyde/PBS, paraffin-embedded lung tissues sections using a VectastainABC kit. Sections 5 uM thick were mounted on APES (aminopropyltriethoxy silane solution)-coated slides, deparaffinized with HistoClear (National Diagnostics, Atlanta, GA) and hydrated in a graded ethanol series. Antigen retrieval was performed using 1 mM Tris-EDTA pH 9.0. Endogenous peroxidase was blocked by hydrogen peroxide. Sections were blocked in normal horse serum. Sections were incubated overnight at 4 °C with antibodies against CD45 at a dilution of 1:200. Secondary ImmPRESS IgG polymer (Vector) was used for a subsequent 30 min incubation. Immunoreactivity was visualized with diaminobenzidine (Vector Laboratories, Burlingame, CA), and sections were counterstained with hematoxylin. Images were collected using an Olympus (BH-2) microscope.

Immunofluorescence

Immunofluorescence was performed on 4 % paraformaldehyde/PBS, paraffin-embedded lung tissues sections. Sections 5 uM thick were mounted on APES (aminopropyltriethoxy silane solution)-coated slides, deparaffinized with HistoClear (National Diagnostics, Atlanta, GA) and hydrated in a graded ethanol series. Antigen retrieval was performed using 1 mM Tris-EDTA pH 9.0. Endogenous peroxidase was blocked by hydrogen peroxide. Sections were then blocke in BLOXALL (Vector Laboratories, Burlingame, CA), followed by 2.5% normal horse serum. Goat anti-mouse Col1 (Southern Biotech,

Birmingham, AL), was used at a dilution of 1:2000. Appropriate Vector HRP-ImmPRESS Polymers (goat) were used to detect primary antibodies, following fluorescent CF dye tyramide conjugates for tyramide signal amplification (Biotium, Fremont, CA): CF594 tyramide. Quenching was achieved using hyfrogen peroxide. Coverslips were mounted with Vectashield with DAPI (Vector Laboratories, Burlingame, CA) and slides were imaged using the Olympus FlouView FV10i confocal microscope (Olympus, Waltham, MA).

Lung Dissociation for Flow Cytometry

Before harvesting, lungs were perfused through the right ventricle to remove erythrocytes. Following harvest, the left lobes of the lungs were washed in 1X PBS and dissociated using the MACs Lung Dissociation Kit (Miltenyi Biotec 130-095-927, Gladbach, Germany) according to the manufacturer's protocol. Briefly, the lung was mechanically disrupted using the gentleMACS dissociator and incubated in a buffer-enzyme mix at 37 °C for 30 min. Following a secondary mechanical disruption with the gentleMACS dissociator, samples were filtered and subjected to ACK lysis buffer (Gibco) to remove remaining erythrocytes. Samples were washed twice in 1X PBS containing 2 % FBS, and resuspended in 1X PBS.

FACs Analysis

Cells were counted and stained with directly conjugated monoclonal anti-mouse antibodies against CD8, CD4, CD11b, CD11c, B220, and F4/80. All stains were performed with isotype controls. Flow cytometry was performed on the LSRII cytometer (BD), and data were analyzed from 250,000 gated events using FlowJo.

Subsection One (such as Statistical Analyses)

Prism 8 (GraphPad) was used for all statistical analysis. Data analysis was done using a Mann-Whitney or unpaired T-test to compare two groups, with a level of significance of $\alpha=0.05$.

Table 1. Mouse qPCR Primers

Gene Name	Forward Primer	Reverse Primer
αSMA	CCCACCCAGAGTGGAGAA	ACATAGCTGGAGCAGCGTCT
β-actin	CTAAGGCCAACCGTGAAAAG	ACCAGAGGCATACAGGGACA
CCL2	CATCCACGTGTTGGCTCA	GATCATCTTGCTGGTGAATGAGT
CCL7	TTCTGTGCCTGCTGCTCATA	TTGACATAGCAGCATGTGGAT
CTGF	CTGCAGACTGGAGAAGCAGA	GATGCACTTTTTGCCCTTCTT
CD163	TCTCAGTGCCTCTGCTGTCA	CGCCAGTCTCAGTTCCTTCT
Col1α1	GCCAAGAAGACATCCCTGAAG	TGTGGCAGATACAGATCAAGC
Col3α1	TTTGTGCAAGTGGAACCTG	TGGACTGCTGTGCCAAAATA
Col5α1	GGACTAGTCCGCTCCCTGTCA ACTTG	GTGGTCACTGCGGCTGAGGA ACTTC
CX3CL1	CGCGTTCTTCCATTTGTGTA	CATGATTTCGCATTTCGTCA
CXCL1	AGACTCCAGCCACACTCCAA	TGACAGCGCAGCTCATTG
CXCL10	TCTCACTGGCCCGTCATC	GCTGCCGTCATTTTCTGC
FGFR1	TCTGGCCTCTACGCTTGC	AGGATGGGAGTGCATCTGAG
Fli1	AATAGCTACATGGATGAGAA GAACG	GTCGAACGTGCTCCTGTGT
HIF1α	GAGCAACTACCTGTTCACCAAA	GGGATTTCTCCTTCCTCAGC
HIF1β	TGCCTCATCTGGTACTGCTG	TGTCCTGTGGTCTGTCCAGT
IFI44	CTGATTACAAAAGAGACATGAC AGAC	AGGCAAAACCAAAGACTCCA
IFNβ	CTGGCTTCCATCATGAACAA	AGAGGGCTGTGGTGGAGAA
IL1β	AGTTGACGGACCCCAAAAG	AGCTGGATGCTCTCATCAGG
IL6	GCTACCAAACTGGATATAATC AGGA	CCAGGTAGCTATGGTACTC CAGAA
IL10	CAGAGCCACATGCTCCTAGA	TGTCCAGCTGGTCCTTTGTT
MMP12	TGATGCTGTCACAACAGTGG	GTAATGTTGGTGGCTGGACTC
MMP9	ACGACATAGACGGCATCCA	GCTGTGGTTCAGTTGTGGTG
MX1	GGGTAGCCACTGGACAGACT	GGCTCTCACAGCTTCTTGCT
PDGFRα	GGAGGAGACAGATGTGAGGTG	GGAGGAGAACAAAGACCGCA
PDGFRβ	TTGCAACGAGAAAGCCGGA	CTATCTACCCACTCGCTCGC
TGFβ1	TGGAGCAACATGTGGAACTC	CAGCAGCCGGTTACCAAG
TGFβ2	TGGAGTTCAGACACTCAACACA	AAGCTTCGGGATTTATGGTGT
TGFβ3	CCCTGGACACCAATTACTGC	TCAATATAAAGGGGGCGTACA
TIMP1	GCAAAGAGCTTTCTCAAAGAC	AGGGATAGATAAACAGGGAAAC ACT
TNFα	TCTTCTCATTCCTGCTTGTGG	GGTCTGGGCCATAGAACTGA

RESULTS

Generation of Fli1$^{flox/flox}$ CAG Cre Mice

Our goal was to generate a viable and fertile transgenic mouse model that, upon controlled induction, resulted in the global deletion of Fli1. Mice expressing Cre recombinase under the chicken β-actin promoter coupled with the cytomegalovirus immediate-early enhancer were purchased from the Jackson Laboratory. When the CAG Cre mice are bred with mice containing loxP-flanked sequences, in this case exon 3 of Fli1, inducible Cre-mediated recombination results in the deletion of functional Fli1 in widespread cells and tissues. Several crosses were needed to generate experimental mice (figure 5B); first, homozygous floxed Fli1 mice were bred with a mouse heterozygous for the CAG Cre transgene.

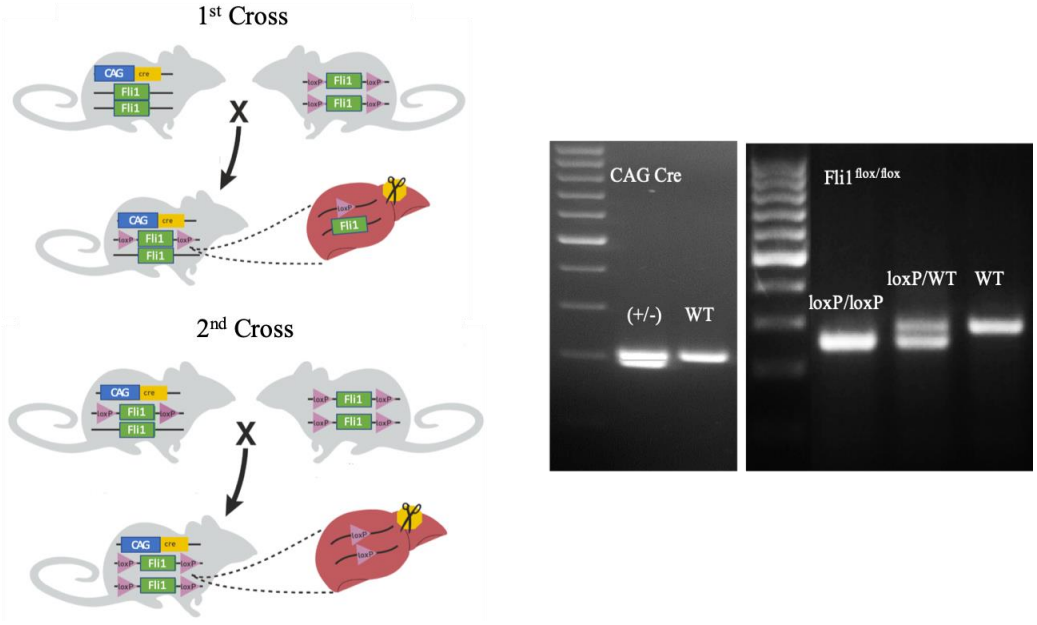

Figure 5: Fli1$^{loxP/loxP}$ CAG Cre Mouse Generation Breeding scheme to generate floxed Fli1 mice (modified from Jackson Laboratories)(left panel); genotyping results for CAG Cre and Fli1$^{flox/flox}$,labels indicate band meaning

Mice heterozygous for a floxed Fli1 allele and heterozygous for the CAG Cre transgene were bred with mice that were homozygous for floxed Fli1. Approximately 25% of the progeny from this cross resulted in mice homozygous for floxed Fli1 and heterozygous for CAG Cre. Mice with this genotype were considered experimental mice; mice homozygous for CAG Cre are not viable or fertile. Genotypes for floxed Fli1 and CAG Cre were confirmed by southern blot (figure 5). 4 weeks and 8 weeks after the final tamoxifen injection, mice were euthanized and Fli1 protein and mRNA expression were evaluated in different tissues to ensure efficient deletion of Fli1.

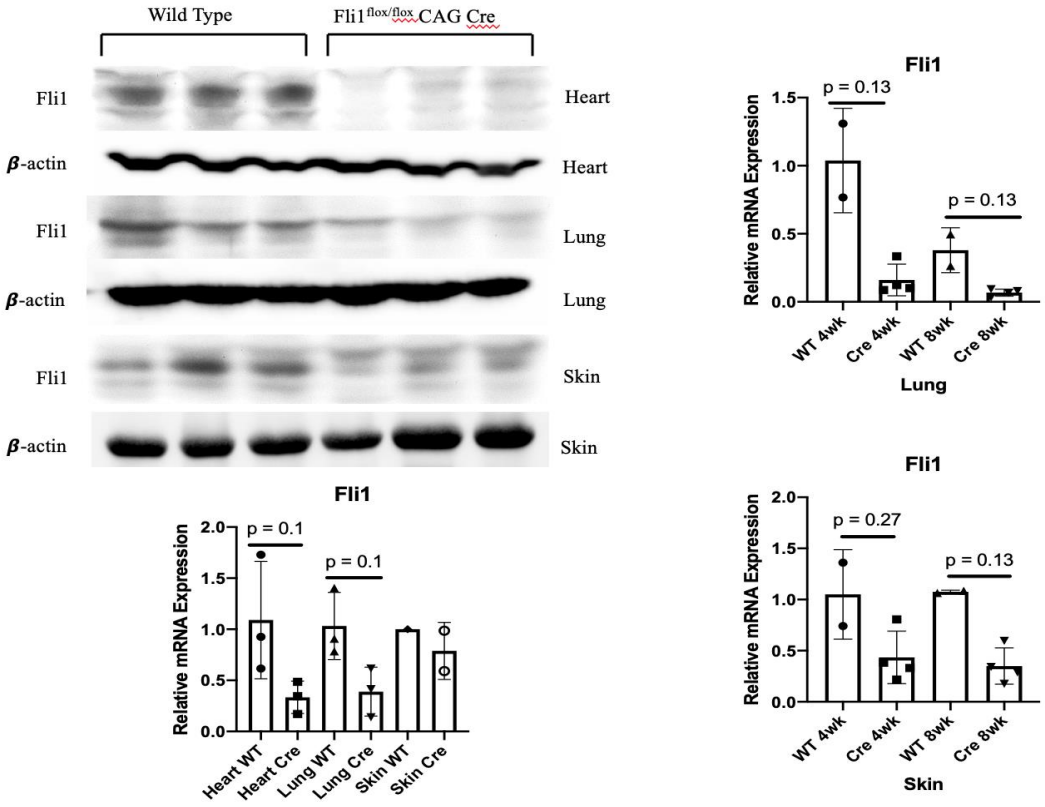

Figure 6: Fli1 Expression Fli1 protein expression (left panel) and relative mRNA expression from whole tissue extracts from the heart, lung, and skin 10 days after Cre induction. Fli1 relative mRNA expression (right panel) from whole tissue extracts from the lung and skin 4 weeks and 8 weeks after Cre induction All data shown as mean ±SD. Non-parametric Mann-Whitney test was used for statistical analysis. *P<0.05, **P<0.01

In a preliminary experiment, CAG Cre showed the most Fli1 loss in the lung and heart tissue, with both the protein and gene expression of Fli1 being reduced in experimental mice. In a subsequent experiment, Fli1 deletion was evaluated 4 and 8 weeks after the tamoxifen injection series (figure 6). Fli1 gene expression was decreased at both 4 and 8 weeks in both the skin and lungs following Cre induction; however, depletion of Fli1 protein expression in these tissues could not be confirmed in all mice, which contributed to much of the variability seen within groups.

Vasculopathy in Fli1$^{flox/flox}$ CAG Cre Mice

To determine whether the postnatal loss of Fli1 in endothelial cells promotes fragile vascular networks, an assay was performed using Evans Blue. After 10 days (figure 7) and 4 weeks (data not shown), mice with global Fli1 deletion showed in increase in vascular permeability (figure 7B) when compared to wild type littermate controls (figure 7A). All experimental mice developed this vascular phenotype.

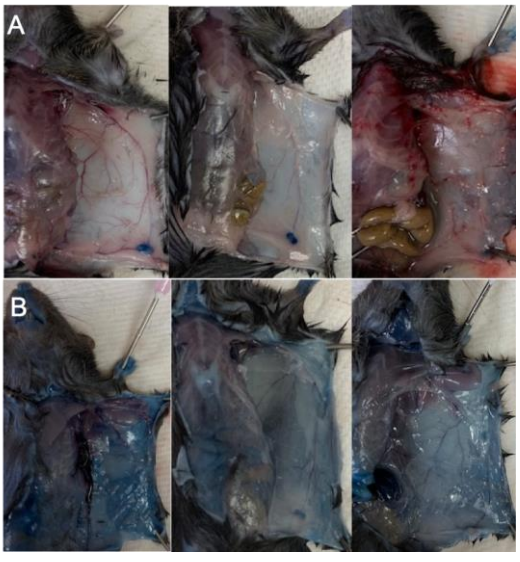

Figure 7: Vessel Permeability with Evans Blue (A) Fli1$^{flox/flox}$ mice with no Cre transgene (WT) 10 days after Cre induction (B) Fli1$^{flox.flox}$ mice with the CAG Cre transgene 10 days after Cre induction

Fibrosis in Fli1$^{flox/flox}$ CAG Cre Mice

To determine if postnatal global loss of Fli1 led to fibrosis in the skin of our experimental mice, a trichrome stain was performed to evaluate collagen architecture and deposition in the dermis (figure 8).

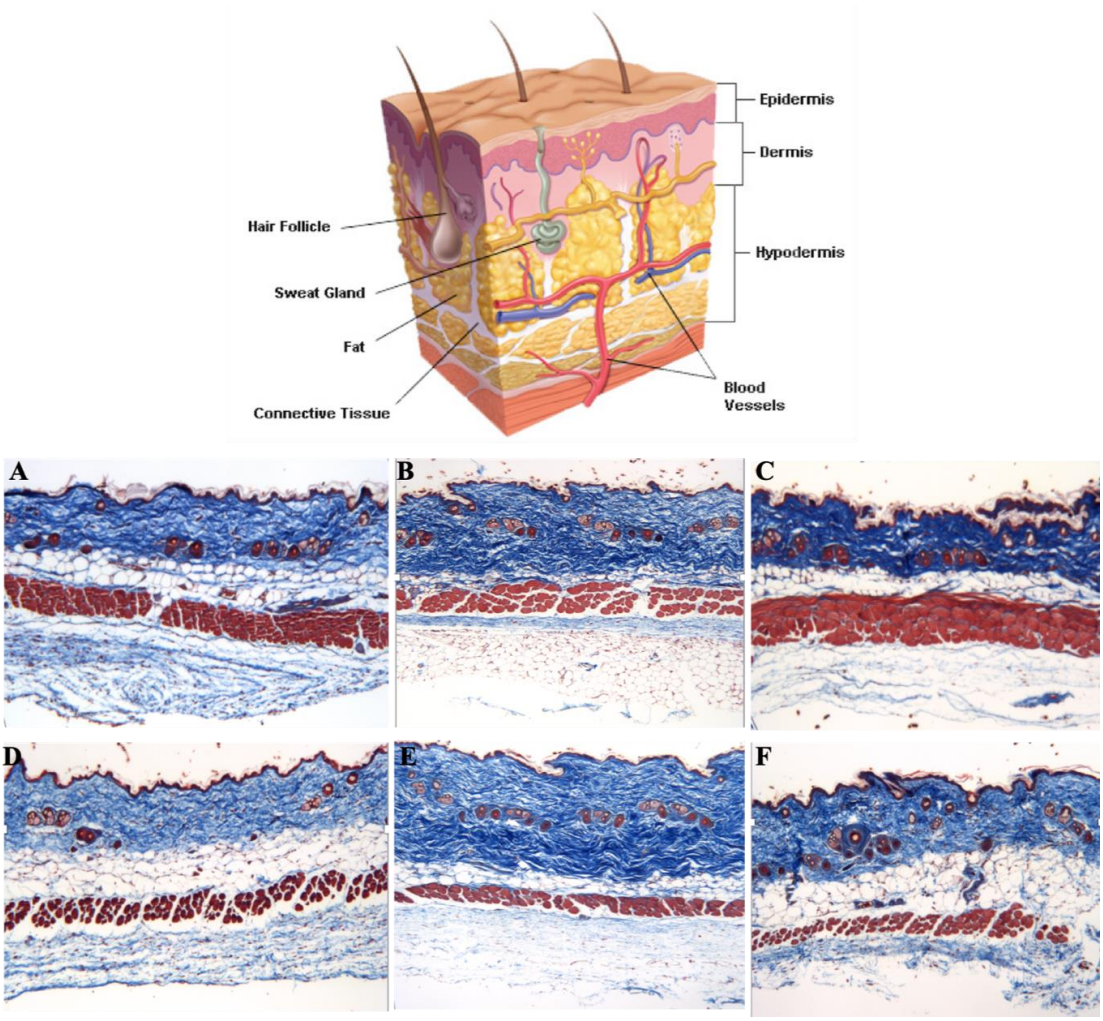

Figure 8: Trichrome and Skin Upper panel represents the structure of normal healthy skin. Lower panel shows trichrome stain in mouse skin [Madhero 88 and M.Komorniczak – CC-BY-3.0] (A) Mouse 2, wild-type skin 4 weeks after Cre induction (B) Mouse 1 Fli1$^{flox/flox}$ CAG Cre skin 4 weeks after Cre induction (C) Mouse 6, Fli1$^{flox/flox}$ CAG Cre skin 4 weeks after Cre induction (D) Mouse 8, wild-type skin 8 weeks after Cre induction (E) Mouse 9, Fli1$^{flox/flox}$ CAG Cre skin 8 weeks after Cre induction 4x (F) Mouse 11, Fli1$^{flox/flox}$ CAG Cre skin 8 weeks after Cre induction 4x

Wild-type mice had a preserved dermal adipose layer 4 weeks (figure 8A) and 8 weeks (figure 8D) after Cre induction. In the experimental group, mice 1, 3, and 6 had the greatest Fli1 deletion in the skin after 4 weeks; however, although there were similar levels of Fli1 deletion in this group mouse 1 exhibited a loss of the dermal adipose layer and thickening of the dermis (figure 8B), while mouse 6 developed densely packed collagen bundles (figure 8C). After 8 weeks, experimental mice 9, and 11 had the most Fli1 deletion at the mRNA level; mouse 9 showed some thickening of the epidermis (figure 8E) while some collagen deposition within the dermal adipose tissue was observed in mouse 11 (figure 8F), indicating that activated fibroblasts may be present, or EndoMT could be occurring within the dermis. 50% of mice developed evidence of fibrosis in the skin.

Real-time PCRs were performed to determine how Fli1 deficiency affects profibrotic gene expression in the skin (figure 9). There were no significant changes in profibrotic gene expression in the skin after 4 or 8 weeks. Matrix metalloproteinase expression was unchanged in the skin of experimental mice compared to controls; however, TIMP1 was increased at both 4 weeks and 8 weeks after Cre induction, supporting the deposition of ECM by inhibiting metalloproteinases in the skin. CD163 was increased 4 weeks and 8 weeks, suggesting the presence of profibrotic macrophages [19]. There was a slight increase in TGF-β3 and Col5α1, but no significant or striking changes in other profibrotic gene expression in the skin when compared to wild-type controls. Interestingly, several mice showed increased expression of PDGFRα and PDGFRβ, which have been correlated with activated fibrotic markers in the skin of SSc

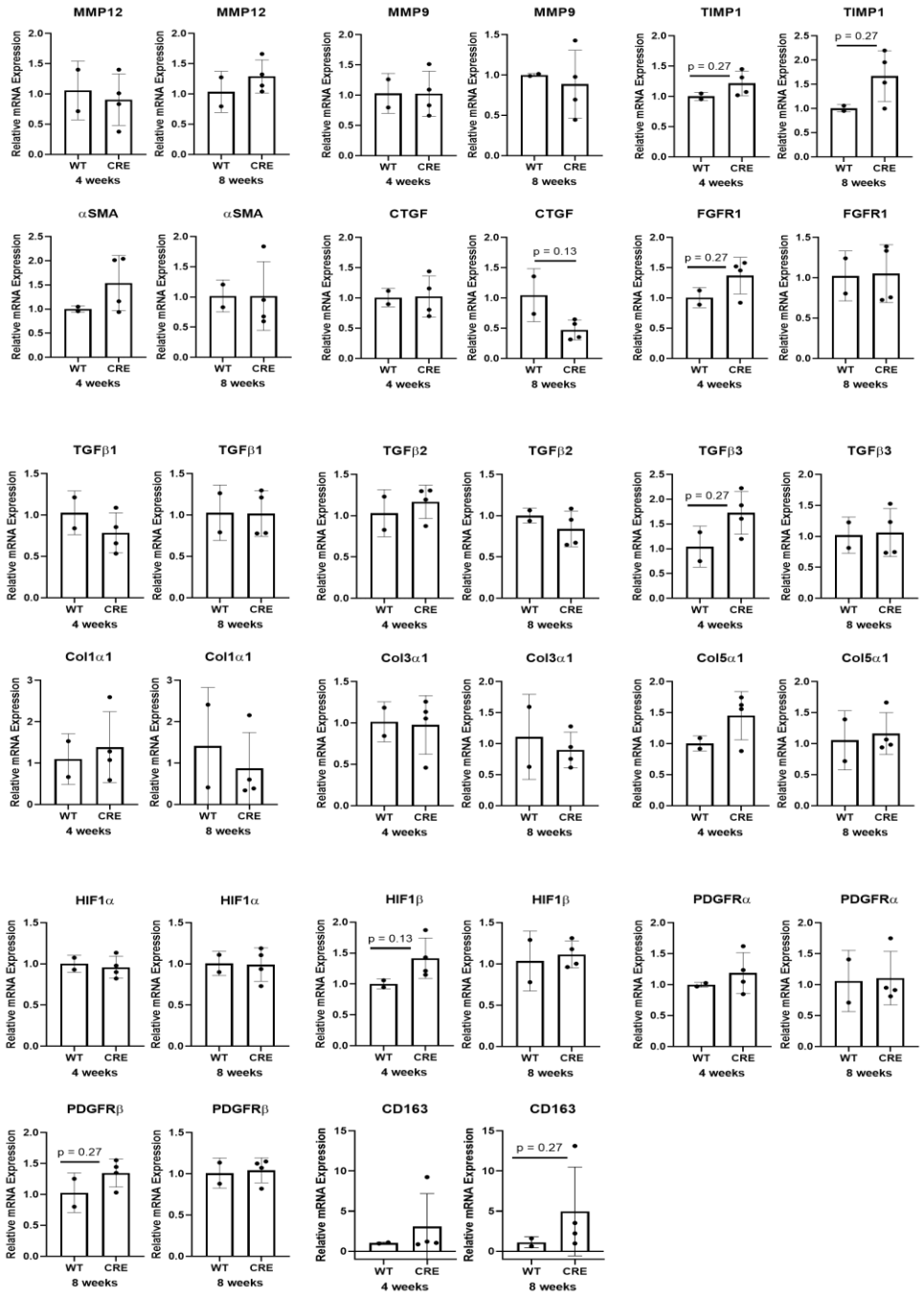

Figure 9: Profibrotic gene expression in the Skin After 4 weeks and 8 weeks, loss of Fli1 in widespread cells and tissues modulates expression of profibrotic genes in the skin. Relative mRNA expression was determined by quantitative RT-PCR. n=1 independent experiment. All data shown as mean ±SD. Non-parametric Mann-Whitney test was used for statistical analysis. *P<0.05, **P<0.01

patients [2]. HIF1β, was also increased after 4 weeks in experimental mice suggesting signs of hypoxia due to vessel rarefaction in the skin. Relative mRNA expression of profibrotic genes may need to be evaluated before there is histological evidence of fibrosis to detect changes in relative mRNA expression between groups.

To determine if a fibrotic phenotype was limited to the skin, a trichrome stain was performed in the lungs (figure 10). Compared to wild-type controls, experimental mice had collagen deposition in perivascular regions surrounding larger bronchi and smaller vessels 4 weeks after Fli1 deletion. 50 % of mice developed fibrosis in bronchovascular units. Mouse 6 developed fibrosis in the skin (figure 8C) and in the lungs (figure 10D) after 4 weeks. Mouse 5 had comparable levels of Fli1 expression, but only developed collagen deposition around small vessels in the lung (figure 10C), while the skin was unaffected. After 8 weeks, the lungs of experimental mice resembled the wild type control mice (data not shown) with no evidence of collagen deposition.

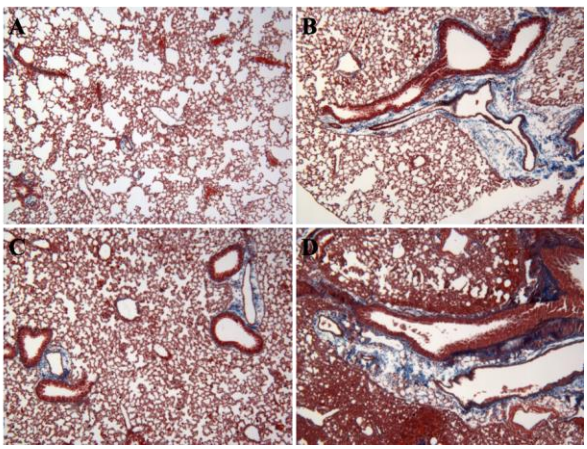

Figure 10: Trichrome in the Lung (A) Mouse 2, wild-type lung 4 weeks after tamoxifen injections. (B) Mouse 3, $Fli1^{flox/flox}$ CAG Cre lung 4 weeks after Cre induction (C) Mouse 5, $Fli1^{flox/flox}$ CAG Cre lung 4 weeks after Cre induction (D) Mouse 6, $Fli1^{flox/flox}$ CAG Cre lung 4 weeks after Cre induction 4X

Profibrotic gene expression was evaluated in the lungs (figure 11). MMP12 was significantly increased after 4 weeks and continued to be elevated in mice after 8 weeks.

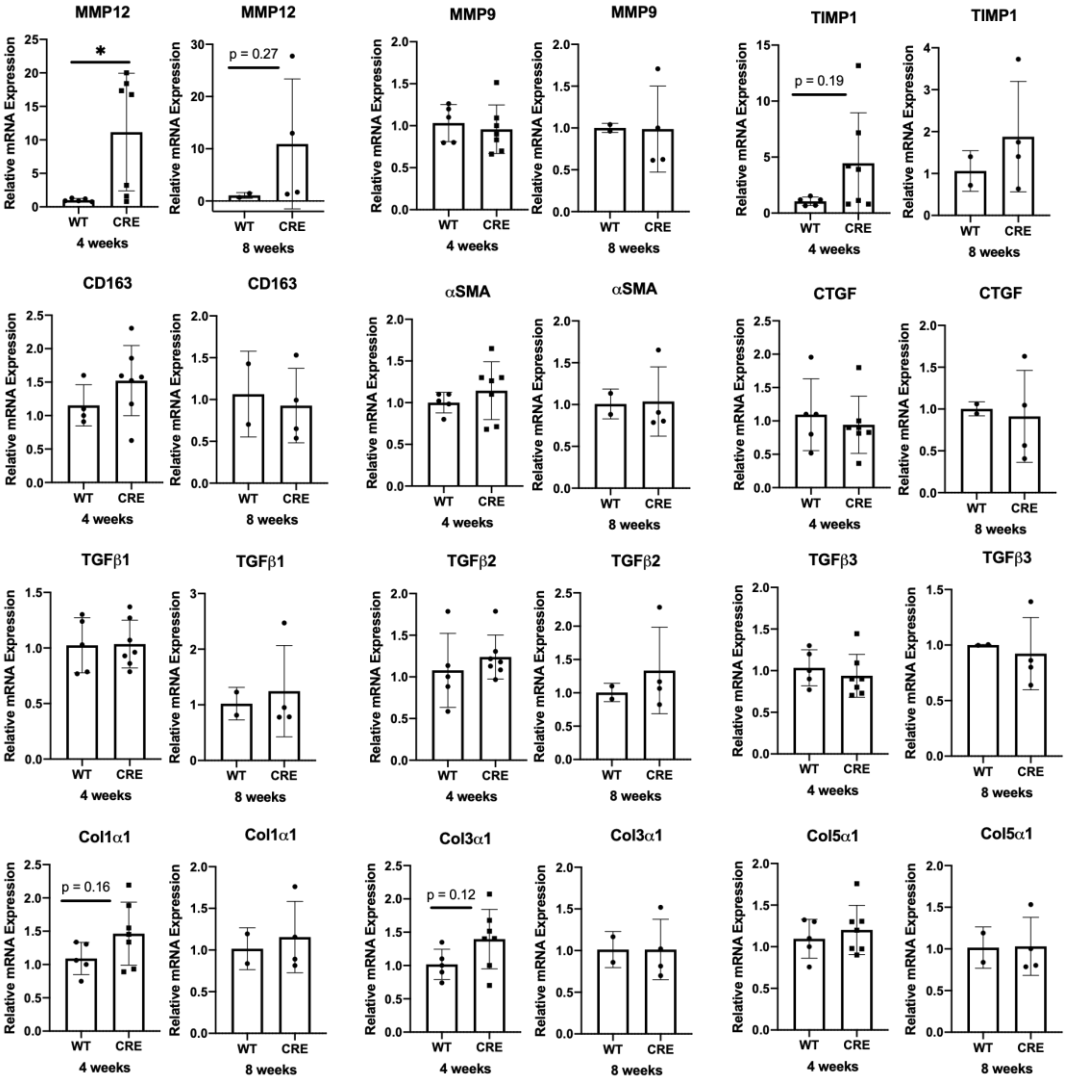

Figure 11: Profibrotic gene expression in the Lung After 4 weeks and 8 weeks, loss of Fli1 in widespread cells and tissues modulates expression of some profibrotic genes in the skin. Relative mRNA expression was determined by quantitative RT-PCR. n=2 independent experiments. All data shown as mean ±SD. Non-parametric Mann-Whitney test was used for 8 week statistical analysis; unpaired t-test was used for 4 week analysis. *P<0.05, **P<0.01

TIMP1, Col1α1, and Col3α1 were increased after 4 weeks in experimental mice, providing more evidence of a profibrotic program in the lungs after 4 weeks. CD163,

although not significant trended toward increase after 4 weeks, suggesting the presence of profibrotic macrophages in the lungs. After 8 weeks, several mice showed elevated MMP12 and TIMP1 expression, indicating sustained activation of mechanisms responsible for sustained ECM remodeling even though fibrosis was not observed in the lungs after 8 weeks in a trichrome stain (data not shown).

To determine if fibrosis developed in the heart of our mice, we performed a picrosirius red stain in the heart 4 weeks after Cre induction (figure 12). There was no pathologic collagen deposition in the hearts of experimental mice when compared to wild-type controls. These mice do not develop fibrosis in the heart after 4 weeks of Fli1 deficiency. The heart was not evaluated after 8 weeks, but heart involvement would be expected in later stages of disease. Experimental mice may require a prolonged pathologic phenotype and additional injury before there is heart involvement.

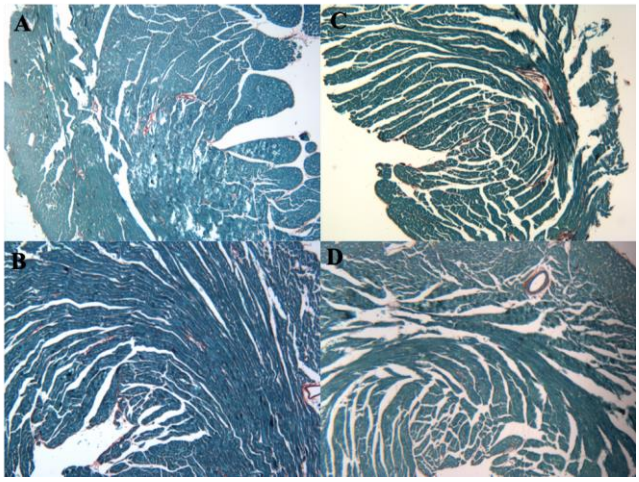

Figure 12: Picrosirius Red Stain in the Heart A and B) Wild-type heart 4 weeks after tamoxifen injections. B and C) $Fli1^{flox/flox}$ CAG Cre heart 4 weeks after Cre induction 4X

Immune dysregulation in Fli1$^{flox/flox}$ CAG Cre Mice

To evaluate immune dysfunction in the lungs, a hematoxylin and eosin (H&E) stain was performed. After 4 weeks of Fli1 downregulation, experimental mice exhibited marked infiltration or proliferation of cells within the alveoli when compared to wild type controls (figure 13). Mouse 6 had the most exacerbated phenotype, exhibiting signs of alveolar hemorrhage and aberrant proliferation (figure 13 C). After 8 weeks, some experimental mice had a decrease in alveolar space, but most mice were comparable to wild-type controls, suggesting there may be a protective restorative mechanism following pulmonary injury in these mice.

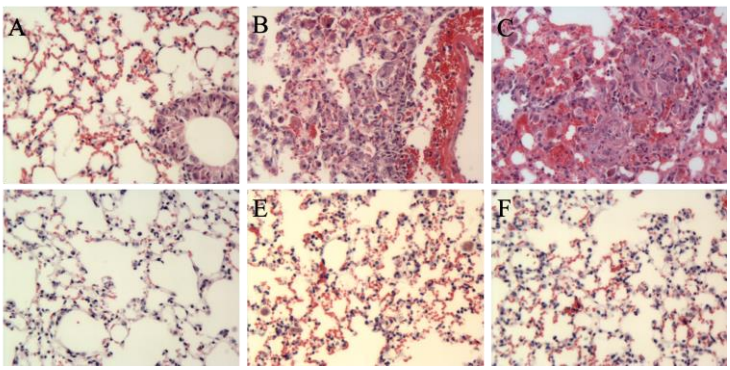

Figure 13: H&E Stain (A) Mouse 2, wild-type lung 4 weeks after tamoxifen injections (B) Mouse 3, Fli1$^{flox/flox}$ CAG Cre lung 4 weeks after Cre induction (C) Mouse 6, Fli1$^{flox/flox}$ CAG Cre lung 4 weeks after Cre induction (D) Mouse 8, wild-type lung 8 weeks after tamoxifen injections (E) Mouse 9, Fli1$^{flox/flox}$ CAG Cre lung 8 weeks after Cre induction (F) Mouse 7, Fli1$^{flox/flox}$ CAG Cre lung 8 weeks after Cre induction. 20x

An immunohistochemical stain using anti-CD45 was done to evaluate leukocyte infiltration to the lung; mouse 5 and 6 had increased leukocyte infiltration (figure 14); however, this was not observed in all experimental mice, and was not statistically significant.

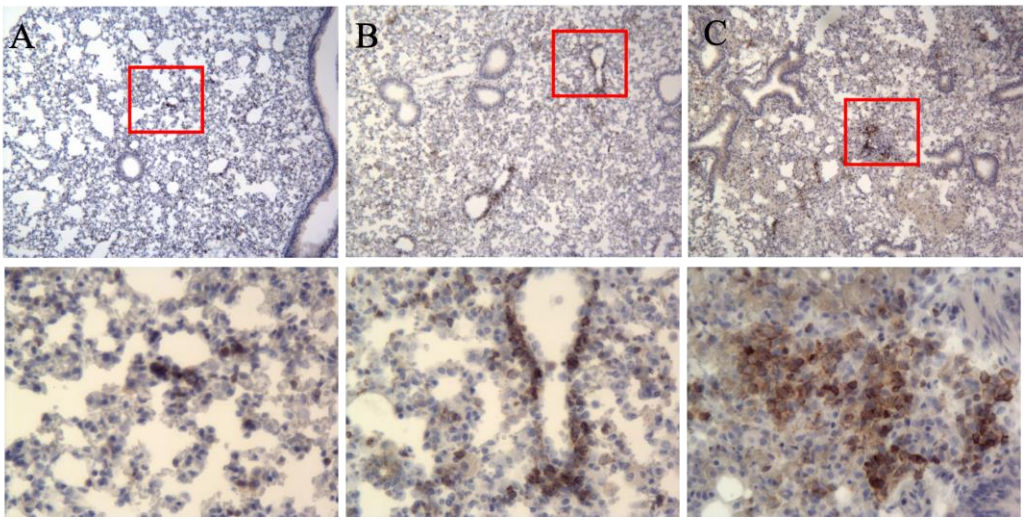

Figure 14: IHC anti-CD45 Lung A) Mouse 2, wild-type lung 4 weeks after tamoxifen injections 4X and 20X. (B) Mouse 5, $Fli1^{flox/flox}$ CAG Cre lung 4 weeks after Cre induction (C) Mouse 6, $Fli1^{flox/flox}$ CAG Cre lung 4 weeks after Cre induction 4X and 20x; red boxes indicate region of 20X image

Flow cytometry was performed to compare immune cell populations in experimental and control mice 8 weeks after Fli1 deletion. In the H&E stain, experimental mice after 8 weeks seemed to have a healthy phenotype in the lungs (figure 13 E-F), but FACs analysis showed experimental mice had increased dendritic cell and macrophage populations, and a decreased B-cell population when compared to wild-type mice (figure 15). These changes may be attributed to loss of Fli1; however, these changes may not be pathologic, but could explain the lack of a profibrotic phenotype 8 weeks after Cre induction. It is interesting that innate antigen presenting cells were increased while adaptive B-cells decreased; however, the B220 epitope that was utilized to identify B-cells in lung cell populations may not be truly representative of that group. In SSc, memory B cells are decreased, but naïve B-cells are increased [24].

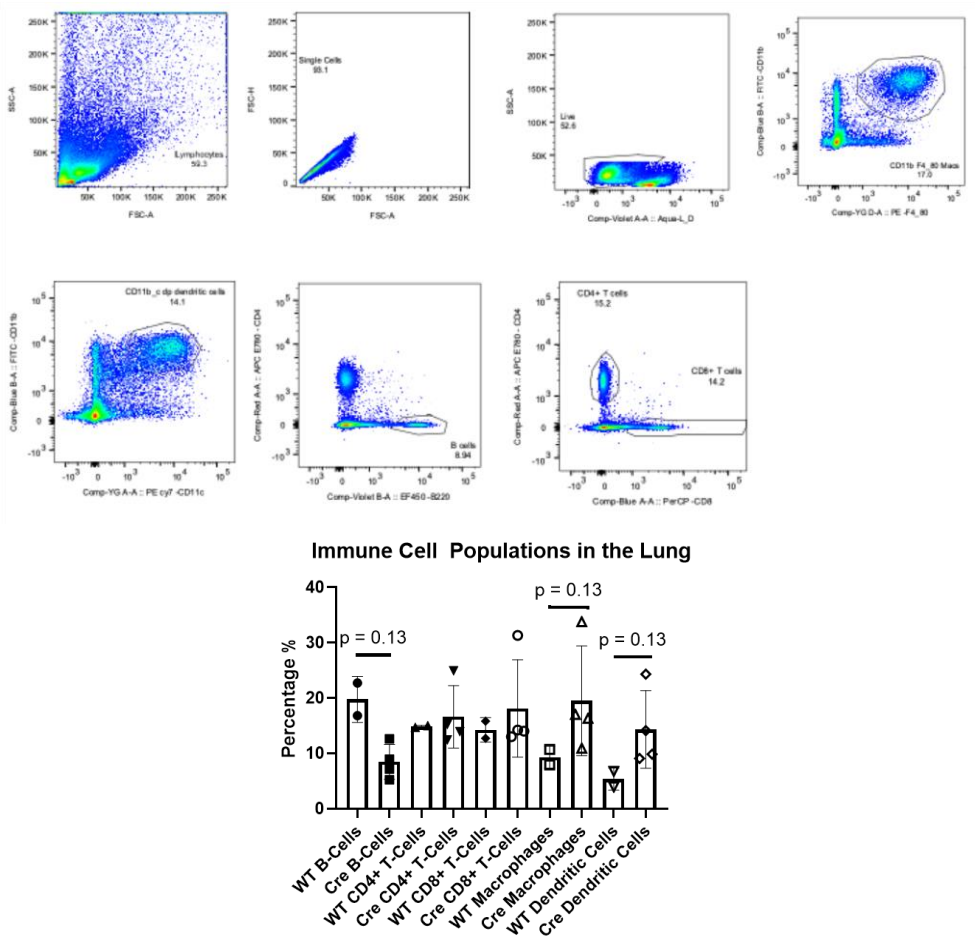

Figure 15: Immune cell populations in the lung Gating strategy for FACs analysis; lymphocyte population, doublets, live/dead, macrophages, dendritic cells, B-cells, CD4+ T-cells and CD8+ T-cells (upper panel); quantification of the cell population by percentage based on 250,000 events. All data shown as mean ±SD. Non-parametric Mann-Whitney test was used for statistical analysis. *P<0.05, **P<0.01

The expression of proinflammatory genes was evaluated in the lungs. The expression of CCL2, TNFα and IFNβ were increased in the lung after 4 weeks, but not 8 weeks (figure 16) suggesting infiltration of monocytes, induction of EndoMT, and provides insight into the inflammatory response, respectively, in early stages. CXCL10 was the markedly increased after 4 weeks and 8 weeks in the lung suggesting a more chronic inflammatory phenotype, with continued monocyte stimulation, and migration of

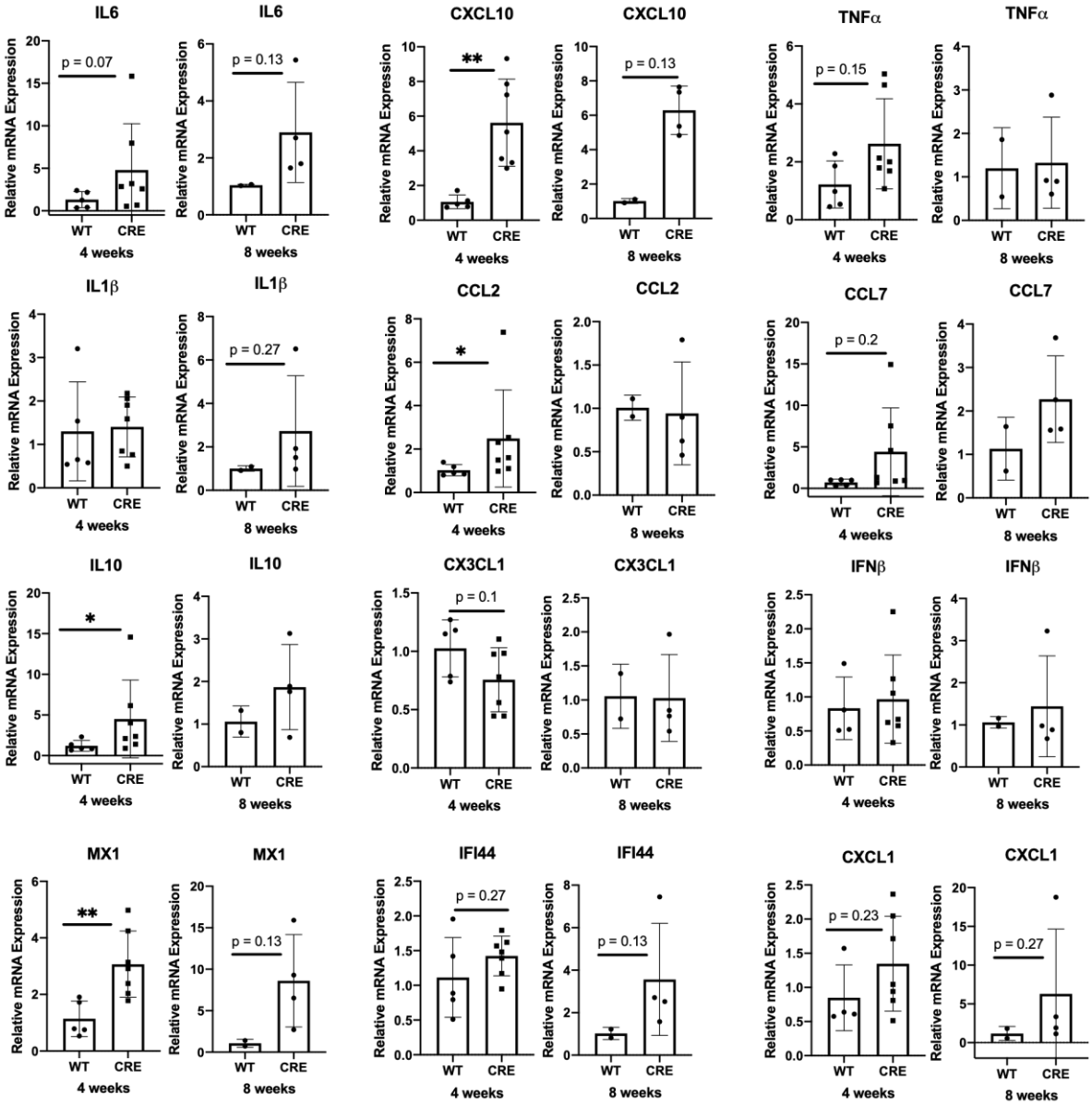

Figure 16: Proinflammatory gene expression in the lung Loss of Fli1 increases inflammatory gene expression after 4 weeks and 8 weeks in the lung. Relative mRNA expression was determined by quantitative RT-PCR. n=2 independent experiments. All data shown as mean ±SD. Non-parametric Mann-Whitney test was used for 8 week statistical analysis; unpaired t-test was used for 4 week analysis. *P<0.05, **P<0.01

other immune cell types to the lung. IFNβ was not significantly increased, but MX1 expression was significantly increased after 4 weeks and continued to be elevated in experimental mice after 8 weeks. In conjunction with increased expression of IL10,

IFI44, CXCL1, CXCL10, and TNFα, this could indicate a type I interferon response [25]. IL-1β expression was increased after 8 weeks, which could mean that activation of the inflammasome pathway also contributes the inflammatory phenotype in these mice.

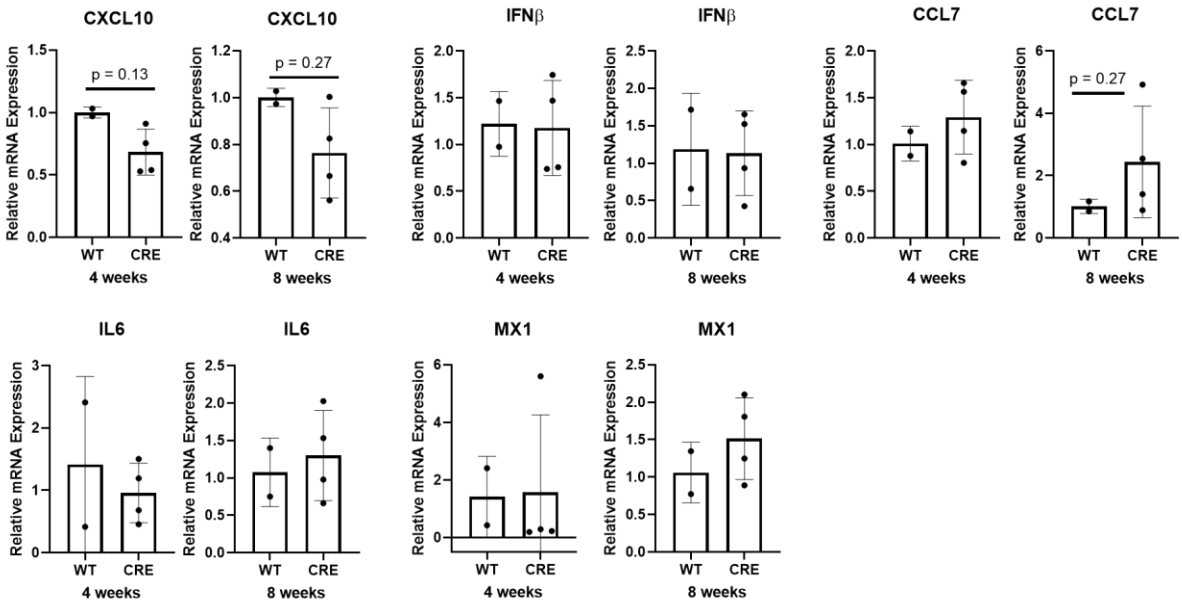

Figure 17: Proinflammatory gene expression in the skin Loss of Fli1 modulates inflammatory genes expression in the skin. Relative mRNA expression was determined by quantitative RT-PCR. n=1 independent experiment. All data shown as mean ±SD. Non-parametric Mann-Whitney test was used for statistical analysis. *P<0.05, **P<0.01

In contrast to the lung, CXCL10 was reduced in the skin both 4 weeks and 8 weeks after Fli1 reduction (figure 17); CXCL10 is increased in the serum and skin of SSc patients [26]. CCL7 was increased after 8 weeks suggesting the presence of activated profibrotic macrophages in the skin. There was much variability within groups; however, mice that developed fibrosis in the skin also had higher levels of proinflammatory gene expression. Interestingly, IFNβ was reduced after 4 weeks and 8 weeks, while MX1 was increased after 8 weeks. For gene expression statistical analysis in the skin, 2 mice were

used in the wild-type control groups, while 4 mice were used in experimental groups. For gene expression statistical analysis in the lung, 5 mice were used in the 4 week control group, 7 mice were used in the 4 week experimental group, 2 mice were used in the 8 week control group, and 4 mice were used in the 8 week experimental group.

After 5 months of Fli1 deletion, mice developed a visible phenotype in the skin (figure 18). Experimental mice had increased hair loss when compared to wild-type controls. Wild-type mice also displayed hair loss suggesting that this is part of the aging process in these mice, but the loss of Fli1 in keratinocytes could be contributing to the phenotype observed in experimental mice. Fli1-deficient keratinocytes have been identified in SSc, and in vivo models have shown that loss of Fli1 in these cells contributes to dermal and esophageal fibrosis [27].

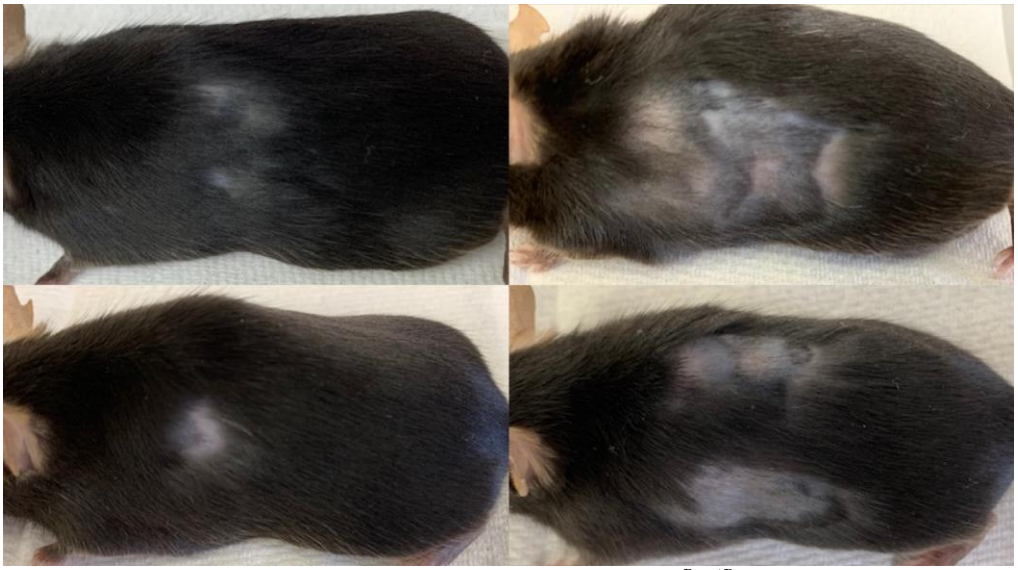

Figure 18: Hair Loss wild-type mice (left panel) and $Fli1^{flox/flox}$ CAG Cre (right panel) 5 months after Cre induction

A trichrome stain was done to compare experimental mice to control mice (figure 19). Areas of hair loss (affected skin) and unaffected skin of experimental mice were used to determine if a fibrotic phenotype persists in the skin after 5 months of Fli1 deletion, and if such a phenotype is limited to areas of hair loss. There was no evidence of fibrosis in these mice; however, affected skin (figure 19D,E) had a decreased number of hair follicles. This pattern of hair loss may be consistent with Alopecia.

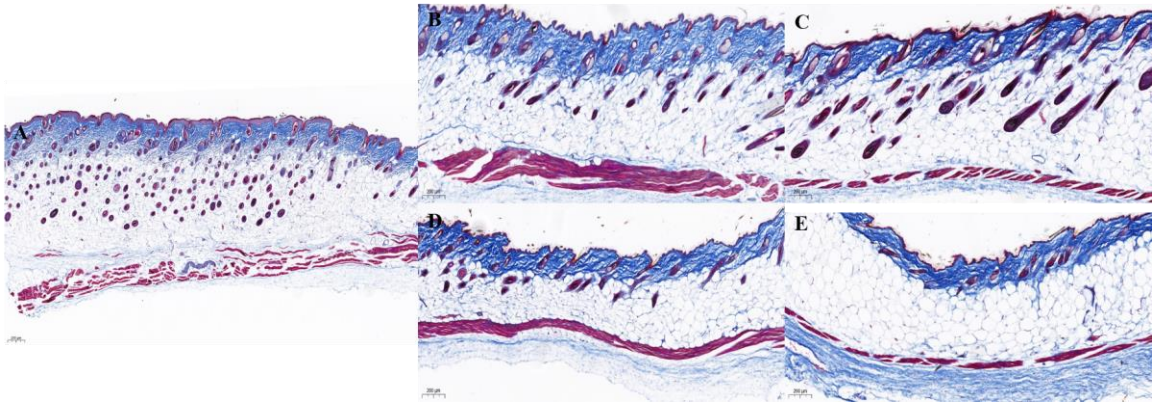

Figure 19: Trichrome in Skin After 5 Months A) Mouse 14 wild-type skin (B) Mouse 15, unaffected $Fli1^{flox/flox}$ CAG Cre skin (C) Mouse 16, unaffected $Fli1^{flox/flox}$ CAG Cre skin (D) Mouse 15, affected $Fli1^{flox/flox}$ CAG Cre skin (E) Mouse 16, affected $Fli1^{flox/flox}$ CAG Cre skin. 4X magnification

To assess skin for inflammatory involvement, an H&E stain was done in skin 5 months after Fli1 deletion (figure 20). There were no significant differences between experimental and control mice, and the typical Alopecia "swarm of bees" pattern of lymphocyte infiltrates [28] surrounding hair follicles was not observed. Inflammation in Alopecia typically occurs during acute stages of the disease and can resolve over time. In later stages of disease, hair loss and accumulation of melanin in the upper dermis can be observed [28]. Although mice seem to develop some irregular pigmentation (figure 18), more experiments are required to definitively characterize the mechanisms behind the

late stage phenotype observed in the skin of experimental mice. The control group also developed some hair loss and pigmentation incontinence, suggesting Fli1 may not be the culprit, but may exacerbate skin involvement over time.

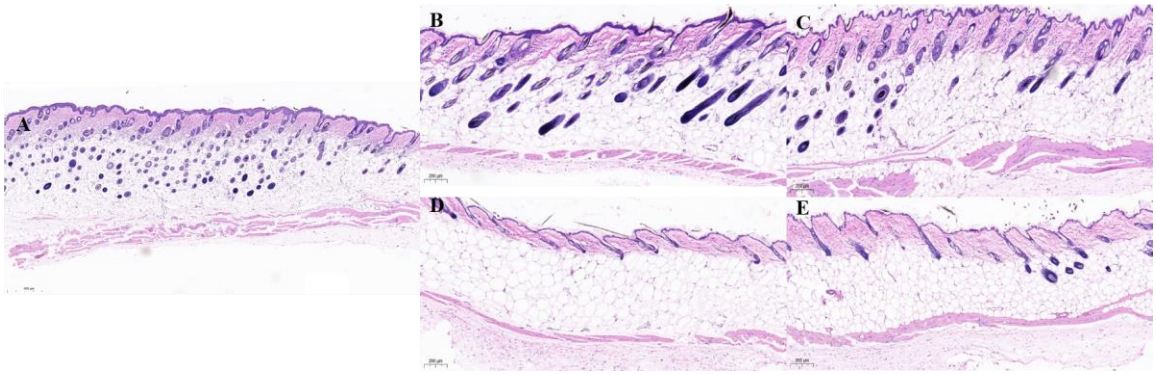

Figure 20: H&E in Skin After 5 Months A) Mouse 14 wild-type skin (B) Mouse 15, unaffected $Fli1^{flox/flox}$ CAG Cre skin (C) Mouse 16, unaffected $Fli1^{flox/flox}$ CAG Cre skin (D) Mouse 15, affected $Fli1^{flox/flox}$ CAG Cre skin (E) Mouse 16, affected $Fli1^{flox/flox}$ CAG Cre skin. 4X magnification

DISCUSSION

Despite the effort committed to elucidating the mechanisms of SSc, effective treatments have not yet been developed. The animal models used to research SSc are not able to capture this complex multi-system disease in one setting, resulting in incomplete characterization of the disease and therapeutics. Here we show a new mouse model that, despite having 50% penetrance of a fibrotic phenotype in our experiments, has the potential to develop many of the systemic effects seen in SSc patients.

All experimental mice developed a vascular phenotype, confirming the effects of Fli1 depletion on endothelial cell injury and the contribution to vascular damage [11]. Endothelial Fli1 serves an essential role in regulating vascular homeostasis including suppression of proinflammatory genes [11]; however, although we observed vasculopathy in the skin of all mice the proinflammatory phenotype was mainly localized in the lungs. An increase in proinflammatory cytokines after 4 weeks and 8 weeks may be evidence of an acute and sustained inflammatory reaction, as there was no difference between wild-type and experimental mice in the H&E stain in the lung after 8 weeks. Flow cytometry showed increased macrophage and dendritic cell populations in the lung after 8 weeks, which could contribute circulating TGFβ [2].

Fli1 haploinsufficiency in a bleomycin-induced skin fibrosis model increased proportions of Th2-like T-regulatory cells, which promote profibrotic macrophage differentiation [29]. In the lungs, but not the skin, CXCL10 gene expression was strikingly increased, possibly contributing to modulation of adhesion molecules and monocyte stimulation, in conjunction with increased CD163 gene expression, confirms a

profibrotic phenotype [20]. CD163 positive cells can be found in both the peripheral blood and in collagen bundles in the skin of SSc patients [20]. Increased gene expression of MX1 and IFI44 suggests a type I interferon induced response. Interferon-β (IFNβ) expression was not increased when Fli1 was depleted, but we did not evaluate interferon-α (IFNα), which has been associated with autoimmune disease by increased levels in the sera of patients with systemic lupus erythematosus (SLE) [25]. A mouse model with targeted MMP12 deletion resulted in a reduction of Fas-induced pulmonary fibrosis [30], suggesting that elevated MMP12 expression may contribute to the fibrotic phenotype in the lungs and skin of floxed Fli1 CAG Cre mice.

Few $Fli1^{flox/flox}$ CAG Cre mice had increased gene expression of TGFβ isoform, major contributors to SSc fibrosis, in the skin and lung [16-18]. Gene expression of α-SMA was increased in both the lungs and skin after 4 weeks, but not 8 weeks, suggesting the presence of activated fibroblasts due to the loss of Fli1 and possible increase of TGFβ [16] in early stages. The 50% of mice with this gene profile developed fibrosis in the skin and the lungs. The gene expression of TGFβ isoforms is not striking and may need to be evaluated before the onset of fibrosis in the skin. The protein level of TGFβ isoforms and collagens was not evaluated and give more insight into these mechanisms. The loss of the adipose tissue layer in the skin of experimental mice is consistent with adipose tissue involvement in the development of fibrotic lesions in SSc [31]. After 5 months of Fli1 deletion, all floxed Fli1 mice expressing CAG Cre exhibited hair loss and pigmentation incontinence. In SSc, hair loss is associated with vessel rarefaction [2]; counting the vessels in the affected skin of experimental mice may be promising.

There was no evidence if heart involvement after 4 weeks in these mice, however myocardial damage is typically secondary to pulmonary hypertension and kidney pathology [32]. Several mice died within a week of the last tamoxifen injection, indicating that the global loss of Fli1 has the potential to develop a fatal phenotype. The cause of death could not be determined, but two mice had enlarged necrotic kidneys. Further experiments utilizing these mice would focus on evaluating the effects of Fli1 deletion in the liver and kidney, investigating gene expression in the skin earlier than 4 weeks after Fli1 deletion, and further characterizing the phenotype in the lungs.

The number of mice used for experiments was limited, and with the heterogeneity within groups, we were only able to observe trends in the lungs and skin. Perhaps by increasing the number of mice per group and performing more experiments the variation seen between wild-type and CAG Cre mice may approach significance. In our experiments, the CAG Cre transgene was active in 4-6 weeks old mice. Beginning tamoxifen injections in younger mice, or in pregnant dames may cause mice to develop a more profound and sustained phenotype. Overall, these mice do not spontaneously develop the triad of SSc clinical manifestations as expected. Genetic predisposition may only be enough to produce a strong vascular phenotype, while a secondary injury may be required to induce systemic effects of Systemic Sclerosis in these mice.

REFERENCES

1. Asano, Y., & Varga, J. (2019). Rationally-based therapeutic disease modification in systemic sclerosis: Novel strategies. *Seminars in Cell & Developmental Biology,* Seminars in cell & developmental biology, 16 December 2019.

2. Varga, J., Trojanowska, M., & Kuwana, M. (2017). Pathogenesis of systemic sclerosis: Recent insights of molecular and cellular mechanisms and therapeutic opportunities. *Journal of Scleroderma and Related Disorders, 2*(3), 137-152.

3. John Varga, & Monique Hinchcliff. (2014). Connective tissue diseases: Systemic sclerosis: Beyond limited and diffuse subsets? *Nature Reviews Rheumatology, 10*(4), 200-202.

4. Bulkley, B H, R L Ridolfi, W R Salyer, and G M Hutchins. "Myocardial Lesions of Progressive Systemic Sclerosis: A Cause of Cardiac Dysfunction." *Circulation* 53.3 (1976): 483-490. Web.

5. Jordan S. Pober, & William C. Sessa. (2007). Evolving functions of endothelial cells in inflammation. *Nature Reviews Immunology, 7*(10), 803-815.

6. Manetti, Mirko, Eloisa Romano, Irene Rosa, Serena Guiducci, Silvia Bellando-Randone, Amato De Paulis, Lidia Ibba-Manneschi, and Marco Matucci-Cerinic. "Endothelial-to-mesenchymal Transition Contributes to Endothelial Dysfunction and Dermal Fibrosis in Systemic Sclerosis." *Annals of the Rheumatic Diseases* 76.5 (2017): 924-934. Web.

7. Spyropoulos, Demetri D., Pharr, Pamela N., Lavenburg, Kim R., Jackers, Pascale, Papas, Takis S., Ogawa, Makio, & Watson, Dennis K. (2000). Hemorrhage, Impaired Hematopoiesis, and Lethality in Mouse Embryos Carrying a Targeted Disruption of the Fli1 Transcription Factor. *Molecular and Cellular Biology, 20*(15), 5643-5652.

8. Gregory M.K. Poon, & Hye Mi Kim. (2017). Signatures of DNA target selectivity by ETS transcription factors. *Transcription*, 8 (3), 193-203.

9. Asano, Yoshihide, Markiewicz, Margaret, Kubo, Masahide, Szalai, Gabor, Watson, Dennis K., & Trojanowska, Maria. (2009). Transcription Factor Fli1 Regulates Collagen Fibrillogenesis in Mouse Skin. *Molecular and Cellular Biology, 29*(2), 425-434.

10. Abedin, M., Nguyen, A., Jiang, N., Perry, C., Shelton, J., Watson, D., & Ferdous, A. (2014). Fli1 acts downstream of Etv2 to govern cell survival and vascular homeostasis via positive autoregulation. *Circulation Research, 114*(11), 1690-9.

11. Asano, Yoshihide, Lukasz Stawski, Faye Hant, Kristin Highland, Richard Silver, Gabor Szalai, Dennis K Watson, and Maria Trojanowska. "Endothelial Fli1 Deficiency Impairs Vascular Homeostasis." *The American Journal of Pathology* 176.4 (2010): 1983-998. Web.

12. Georgiou, Maroulakou, Green, Dantis, Romanospica, Kottaridis, . . . Bhat. (1996). Expression of ets family of genes in systemic lupus erythematosus and Sjogren's syndrome. *International Journal of Oncology, 9*(1), 9-18.

13. Wang, Y., Fan, P., & Kahaleh, B. (2006). Association between enhanced type I collagen expression and epigenetic repression of the FLI1 gene in scleroderma fibroblasts. *Arthritis & Rheumatism, 54*(7), 2271-2279.

14. Taniguchi, Takashi, Miyagawa, Takuya, Toyama, Satoshi, Yamashita, Takashi, Nakamura, Kouki, Saigusa, Ryosuke, . . . Asano, Yoshihide. (2018). CXCL13 produced by macrophages due to Fli1 deficiency may contribute to the development of tissue fibrosis, vasculopathy and immune activation in systemic sclerosis. *Experimental Dermatology, 27*(9), 1030-1037.

15. Czuwara-Ladykowska, J., Shirasaki, F., Jackers, P., Watson, D., & Trojanowska, M. (2001). Fli-1 inhibits collagen type I production in dermal fibroblasts via an Sp1-dependent pathway. *The Journal of Biological Chemistry, 276*(24), 20839-20848.

16. Asano, Y., Bujor, A., & Trojanowska, M. (2010). The impact of Fli1 deficiency on the pathogenesis of systemic sclerosis. *Journal of Dermatological Science, 59*(3), 153-162.

17. Asano, Y., Czuwara, J., & Trojanowska, M. (2007). Transforming growth factor-beta regulates DNA binding activity of transcription factor Fli1 by p300/CREB-binding protein-associated factor-dependent acetylation. *The Journal of Biological Chemistry, 282*(48), 34672-34683

18. Trojanowska, Maria. “Noncanonical transforming growth factor beta signaling in scleroderma fibrosis.” *Current opinion in rheumatology* vol. 21,6 (2009): 623-9.

19. Shapouri-Moghaddam, Abbas, Saeed Mohammadian, Hossein Vazini, Mahdi Taghadosi, Seyed-Alireza Esmaeili, Fatemeh Mardani, Bita Seifi, Asadollah Mohammadi, Jalil T. Afshari, and Amirhossein Sahebkar. "Macrophage

Plasticity, Polarization, and Function in Health and Disease." *Journal of Cellular Physiology* 233.9 (2018): 6425-440. Web.

20. Higashi-Kuwata, Jinnin, Makino, Fukushima, Inoue, Muchemwa, Yonemura, Komohara, Takeya, Mitsuya, and Ihn. "Characterization of Monocyte/macrophage Subsets in the Skin and Peripheral Blood Derived from Patients with Systemic Sclerosis." *Arthritis Research & Therapy* 12.4 (2010): R128. Web.

21. Suzuki, Eiji, Sarah Williams, Shuzo Sato, Gary Gilkeson, Dennis K. Watson, and Xian K. Zhang. "The Transcription Factor F Li-1 Regulates Monocyte, Macrophage and Dendritic Cell Development in Mice." *Immunology* 139.3 (2013): 318-27. Web.

22. Soare, Alina, Andreas Ramming, Jerome Avouac, and Jörg H.W Distler. "Updates on Animal Models of Systemic Sclerosis." *Journal of Scleroderma and Related Disorders* 1.3 (2016): 266-76. Web.

23. Artlett, C. (2014). Animal models of systemic sclerosis: Their utility and limitations. *Open Access Rheumatology : Research and Reviews, 6*, 65-81.

24. Sato, Shinichi, Manabu Fujimoto, Minoru Hasegawa, and Kazukiko Takehara. "Altered Blood B Lymphocyte Homeostasis in Systemic Sclerosis: Expanded Naive B Cells and Diminished but Activated Memory B Cells." *Arthritis & Rheumatism* 50.6 (2004): 1918-927. Web.

25. Lionel B. Ivashkiv, & Laura T. Donlin. (2013). Regulation of type I interferon responses. *Nature Reviews Immunology*, *14*(1), 36-49.

26. Rabquer, B., Tsou, P., Hou, Y., Thirunavukkarasu, E., Haines, G., Impens, A., . . . Koch, A. (2011). Dysregulated expression of MIG/CXCL9, IP-10/CXCL10 and CXCL16 and their receptors in systemic sclerosis. *Arthritis Research & Therapy*, *13*(1), R18.

27. Takahashi, Asano, Sugawara, Yamashita, Nakamura, Saigusa, . . . Sato. (2017). Epithelial Fli1 deficiency drives systemic autoimmunity and fibrosis: Possible roles in scleroderma. *The Journal of Experimental Medicine, 214*(4), 1129-1151.

28. Darwin, E., Hirt, P., Fertig, R., Doliner, B., Delcanto, G., & Jimenez, J. (2018). Alopecia areata: Review of epidemiology, clinical features, pathogenesis, and new treatment options. *International Journal of Trichology*, *10*(2), 51-60.

29. Saigusa, Asano, Taniguchi, Hirabayashi, Nakamura, Miura, Yamashita, Takahashi, Ichimura, Toyama, Yoshizaki, Trojanowska, and Sato. "Fli1-

haploinsufficient Dermal Fibroblasts Promote Skin-localized Transdifferentiation of Th2-like Regulatory T Cells." *Arthritis Research & Therapy* 20.1 (2018): 23. Web.

30. Matute-Bello, G., Wurfel, M., Lee, J., Park, D., Frevert, C., Madtes, D., . . . Martin, T. (2007). Essential role of MMP-12 in Fas-induced lung fibrosis. *American Journal of Respiratory Cell and Molecular Biology*, *37*(2), 210-21.

31. Kruglikov, I. (2017). Interfacial Adipose Tissue in Systemic Sclerosis. *Current Rheumatology Reports, 19*(1), 1-8.

32. Lambova, S. (2014). Cardiac manifestations in systemic sclerosis. *World Journal of Cardiology, 6*(9), 993-1005.

CURRICULUM VITAE